CHAPTER 6: OHMIC DROP COMPENSATION AND NEGATIVE GLOBAL COUPLING

It has been pointed out that the impact of the coupling conditions on the spatiotemporal dynamics of the oscillatory $Pt|H_2SO_4,Cl^-,Cu^{2+}|H_2$ system is one of the central questions of the present thesis. The systematic study of the impact of the global coupling on dynamic behavior of the $Pt|H_2SO_4,Cl^-,Cu^{2+}|H_2$ system is launched in this chapter.

6.1 INTRODUCTION

As already discussed in chapter 2, under potentiostatic control, whenever part of the cell resistance is compensated, a negative global coupling (NGC) is induced into the system. Experimental results illustrating different manifestations of the NGC in electrochemical systems have been published [40-45]. In all of these reports, experiments were carried out with a Haber-Luggin capillary. Krischer and coworkers [79] have reformulated the term referring to the strength of the NGC entering the equation describing the time evolution of the double layer potential. An important result of this formulation is that independent of how the compensation is achieved, that is whether it is achieved via a Haber-Luggin capillary or via electronic compensation, a NGC is introduced, whose strength depends only on the cell resistance, R_Ω, and the compensated resistance, R_c. In this formulation the evolution equation of the double layer evolution reads,

$$C_{sp}\frac{\partial\phi_{DL}}{\partial t} = -i_F + \frac{U-\phi_{DL}}{A\left(R_\Omega - R_c\right)} - \frac{1}{AR_\Omega}\left(\frac{R_c/R_\Omega}{1-R_c/R_\Omega}\right)\left(\left\langle\phi_{DL}\right\rangle - \phi_{DL}\right) - \sigma\left(\frac{\partial\phi}{\partial z} - \phi\right)\Bigg|_{z=WE} . \quad (6.1)$$

The third term in the right hand side describes the global coupling, and the coefficient

$$\frac{1}{AR_\Omega}\left(\frac{R_c/R_\Omega}{1-R_c/R_\Omega}\right)$$

is the strength of the global coupling.

Realistic three-dimensional simulations for a ring-shaped electrode have confirmed the analytical formulation of the global coupling strength [79]. Figure 6.1 depicts one of these simulations where anti-phase oscillations resulting from the NGC were obtained. Identical patterns were observed for two configurations: (a) when the RE was placed close to the WE, and (b) when the RE was placed far away from the WE and part of the electrolyte resistance was compensated by the an electronic device such that the cell resistance was identical under both conditions.

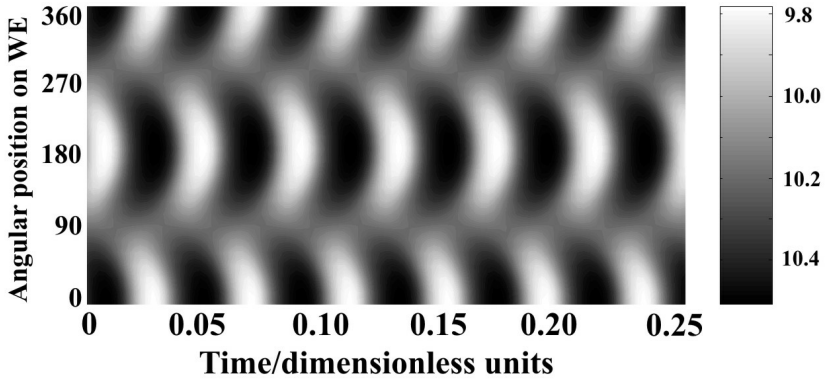

Figure 6.1: Simulated spatiotemporal evolution of the interfacial potential for a ring-shaped WE, in simulations carried out by Dr. A. Bîrzu using a three-dimensional model for metal electrodissolution (see, e.g. [79, 179, 180]). For parameters see ref. [79].

Note that the dynamics is different if the cell resistance is not compensated but reduced by minimizing the distance between CE and WE or by increasing the electrolyte conductivity.

The primary goal of the present chapter is to provide experimental evidence of the fact that the NGC introduced into the system by means of a Haber-Luggin capillary has the same effect as that introduced by electronic compensation. In other words, the two situations theoretically investigated and depicted in Figure 6.1 are experimentally tested. In the next section, problems connected to ohmic drop compensation and the use of a negative impedance device are briefly introduced. Then, the experimental results are presented. The general discussion is given in the subsequent section, and the chapter ends with the summary of the main conclusions.

6.2 OHMIC DROP COMPENSATION AND THE NEGATIVE IMPEDANCE DEVICE (NID)

The fact that the RE can never probe the potential at a point exactly on the border of the double layer [66, 71] implies that some uncompensated resistance, R_u, is left between the actual measured point and the border of the double layer. This point was already discussed in chapter 2 and is schematically shown in Figure 6.2 (a). In this figure, the cell resistance, R_Ω, is partially compensated by placing the RE between the CE and the WE and the compensated resistance, R_c, is given by: $R_\Omega - R_u$. Due to the uncompensated resistance, the applied voltage

U is composed of the potential drop across the double layer and the ohmic drop through the electrolyte, such that: $U = \phi_{DL} + IR_u$.

The first and most common way of compensating the ohmic drop through the electrolyte is by optimizing the electrode arrangement, i.e., reducing, as much as possible, the distance between the RE and the WE by means of a Haber-Luggin capillary [67]. More sophisticated ways of compensating the ohmic drop involve electronic devices and are reviewed in refs. [181, 182]. However, also these devices induce a NGC. It should be emphasized that the NGC is necessarily linked to ohmic drop compensation and to the ratio R_c/R_Ω. Approaching the CE to the WE reduces the R_Ω term, which can be viewed as a way of 'compensation' but does not induce NGC, and the result in the spatiotemporal dynamics is quite different (see the discussion on the effect of the CE/WE separation in chapter 5). For the electronic compensation of the cell resistance, a special device was build because, as already mentioned in the third chapter, the built-in ohmic drop compensation of the potentiostat presently employed has the limitation of the upper limit in the set R_c of 100 Ω and is therefore not suitable for the large resistances present in the studied system. Hence, the approach adopted here in order to surmount this limitation consists of the inclusion of a compensation apparatus, which possesses a negative impedance converter [183, 184] or device (NID), into the cell circuit, but outside the negative feedback loop of the potentiostat. Lamy and Hermann [185] in a very detailed analysis suggest that the NID possesses several advantages, among them the superior stability of the whole cell/regulation system.

Figure 6.2 (b) depicts the NID circuit [185, 186]. The NID is connected between the WE and the potentiostat (ground) and its voltage/current (the *low frequency* input impedance [181, 185]) characteristic is given by $R_{NID} = -R_1(R_2/R_3)$.

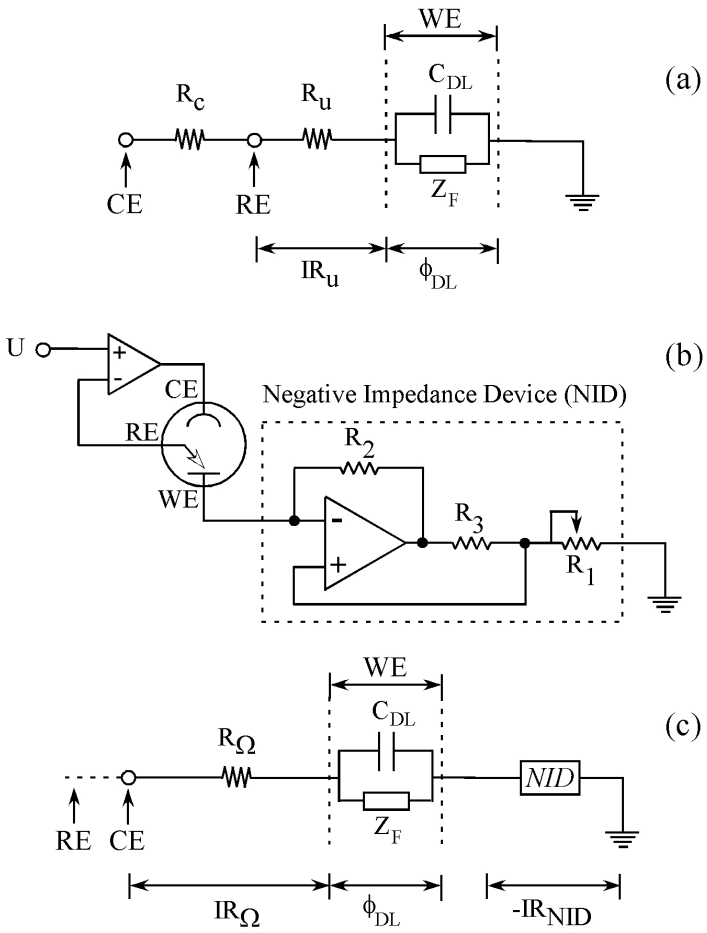

Figure 6.2: (a) General circuit of an electrochemical cell. (b) Schematics of a Negative Impedance Device (NID) connected between the WE and the potentiostat (*ground*). In this scheme, the voltage U is applied by a differential potentiostat. (c) Same circuit as in (a) but now including the NID; here the RE is placed at some point behind the CE.

In the configuration used in the present work (designed by Fritz Haber Electronic Laboratory), $R_2 = R_3 = 1$ kΩ and $R_{NID} = -R_1$. Thus, the whole device acts like a negative impedance at low and moderated frequencies [181] and when connected to an electrochemical cell (Figure 6.2 (c)) the compensated portion of the cell resistance is given by $R_c = -R_{NID}$ ($= R_\Omega - R_u$). In other words, if in Figure 6.2 (c) $-R_{NID}$ is set to the R_c value given in (a), both circuits are equivalent and possess identical load lines: $I = U/R_u - \phi_{DL}/R_u$. This device allows for an easy adjustment of the compensate resistance, and thus provides also an easy way to control the strength of the global coupling.

6.3 RESULTS

An example showing the compensating effect of the NID connected to an electrochemical cell under potentiostatic control is shown in Figure 6.2 (c). Depicted are four different cyclic voltammograms for different R_{NID} values.

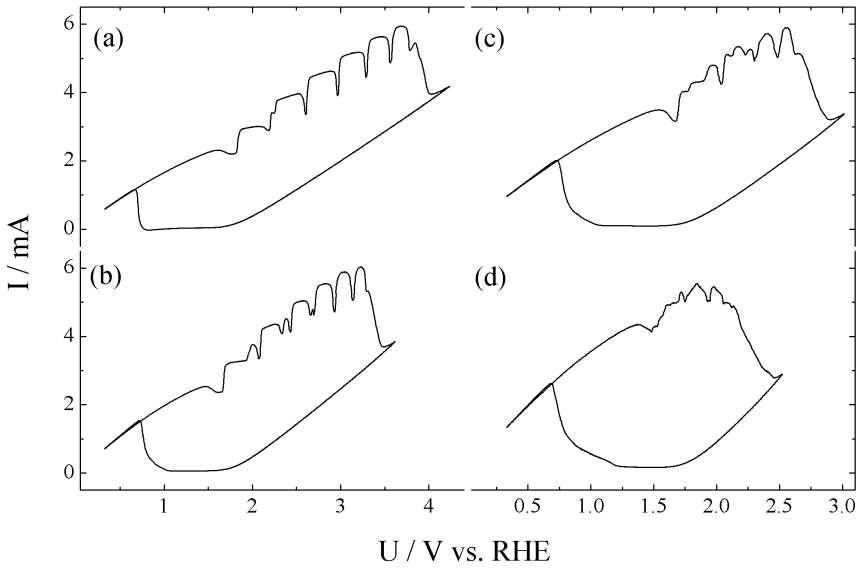

Figure 6.3: Cyclic voltammograms at 0.1 Vs^{-1} of the $Pt|H_2SO_4,Cl^-,Cu^{2+}|H_2$ system. The RE was placed in an external compartment below the plane of the CE and R_{NID} was set to: (a) 0 Ω, (b) –100 Ω, (c) –200 Ω, and (d) –300 Ω. Remaining conditions: R_Ω = 570 ± 10 Ω; Electrolyte: 0.5 mM H_2SO_4, 0.1 mM HCl, and 0.025 mM $CuSO_4$ saturated with H_2. ω = 20 Hz.

As clearly seen in this figure, the effect of ohmic drop compensation is not merely the *quantitative* one due to the reduction of the ohmic drop term of the 'U = ϕ_{DL} – IR_u' constraint. The additional *qualitative* effect on the dynamics of the system can be inferred from the changes in the current/voltage trace, in particular in the oscillatory region and apparently less regular oscillations are seen for higher compensation.

The next step is to proof that the NGC induced when partially compensating the cell resistance does not depend on the way by which the compensation is achieved, provided that the same magnitude is compensated. Figure 6.4 describes the experimental strategy adopted to do so.

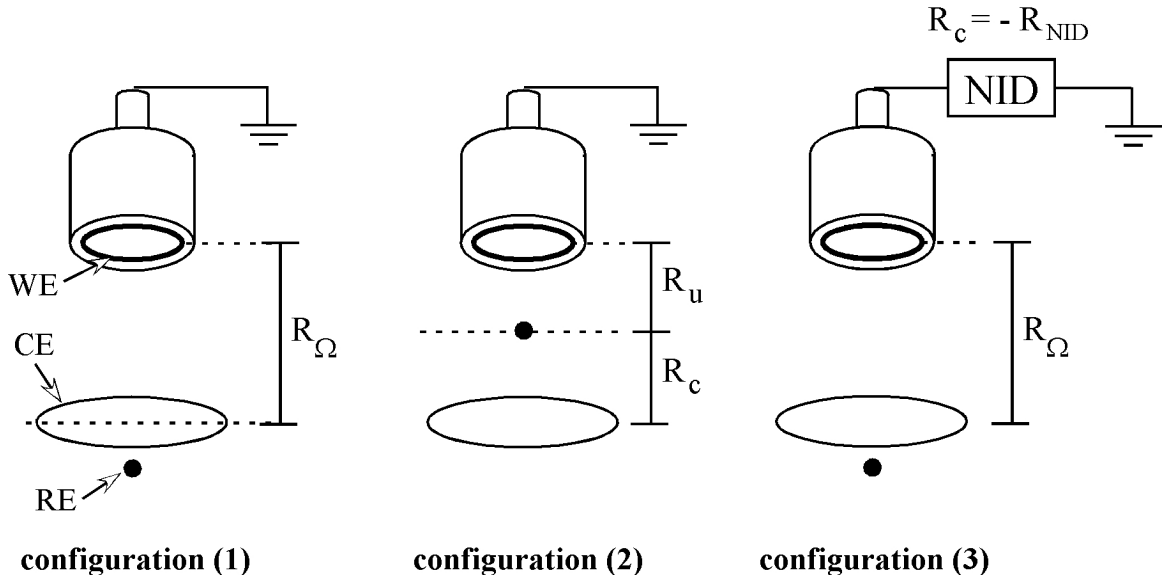

Figure 6.4: Schematics of the different configurations employed. (a) The RE is placed below the CE, no NGC is present and the cell resistance is $R_\Omega = R_u$. (b) The RE is placed above the plane of the CE, compensating the portion R_c of the cell resistance, R_Ω. The resistance left is given by R_u. Note that in (a) and (b) the WE is grounded. (c) The same amount of resistance as in (b) is compensated by the NID.

Details of each configuration are as follows:

Configuration (1): The RE was placed externally to the main cell compartment. The junction between the RE compartment and the main compartment was below the position of the CE plane. Hence, no resistance was compensated (i.e., $R_c = 0$) and $R_u = R_\Omega$ (= 510 ± 10 Ω in the specific case here).

Configuration (2): The RE was put into a J-shaped glass capillary whose tip was placed on the central axis of the ring-shaped WE and 3 mm below the plane of the WE. Here: R_u = 270 ± 10 Ω and $R_c/R_\Omega \approx 0.47$.

Configuration (3): The RE was placed externally to the main cell compartment as in configuration (1) and the NID was inserted between the WE and the ground as given in Figure 6.2 (c). In this case: $R_{NID} = -250$ Ω and $R_u = 260 \pm 10$ Ω, hence $R_c/R_\Omega \approx 0.49$.

The voltammetric response of configuration (1) is depicted in Figure 6.5. To give an idea of the magnitude of the uncompensated cell resistance, $R_u = R_\Omega$, both the I/U (curve *i*) and the I/ϕ_{DL} (curve *ii*) are displayed, where ϕ_{DL} was calculated from $\phi_{DL} = U - IR_\Omega$.

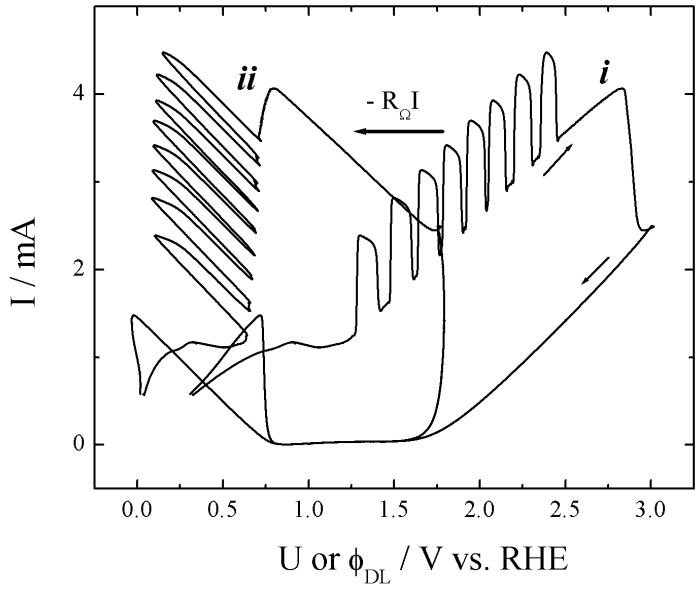

Figure 6.5: Cyclic voltammogram of the $Pt|H_2SO_4,Cl^-,Cu^{2+}|H_2$ system where the current is displayed as a function of the externally applied potential U (curve *i*) and of ϕ_{DL} (curve *ii*), as calculated according to $U = \phi_{DL} - R_\Omega I$, for $R_\Omega = 510\ \Omega$. Experimental conditions: The RE was placed in an external compartment below the plane of the CE (configuration (1)). Electrolyte: 0.5 mM H_2SO_4, 0.1 mM HCl, and 0.05 mM $CuSO_4$ saturated with H_2. $\omega = 20$ Hz.

The oscillatory region in the I/U curve starts during the positive sweep, at around 1.26 V. During the voltage sweep the oscillation frequency and amplitude remain almost constant up to ca. 2.47 V, where a hard bifurcation destroys the limit cycle. Increasing U further, at $U \approx 2.8$ V, the oxide formation blocks the electrode for the HOR, and the residual current at higher potentials is due to the oxygen evolution. This process is seen also in the negative scan such that the current goes to zero only at about 1.8 V. From there on, the current remains close to zero up to the potential at which surface oxides are reduced.

Potentiostatic experiments in the oscillatory region were carried out and the overall behavior was qualitatively identical in the entire voltage region. Typical results are shown in Figure 6.6. Results are given in terms of I(t), $U_{PP}(t)$, and $(U_{PP} - \langle U_{PP} \rangle_x)(t)$, as well as the spatiotemporal evolution of the U_{PP}, and its inhomogeneous part $U_{PP} - \langle U_{PP} \rangle_x$. The large amplitude, relaxation-like current oscillations (Figure 6.6(a)) are characterized by the fast passive/active, i.e., low/high, current transition followed by a relatively long relaxation in the active region.

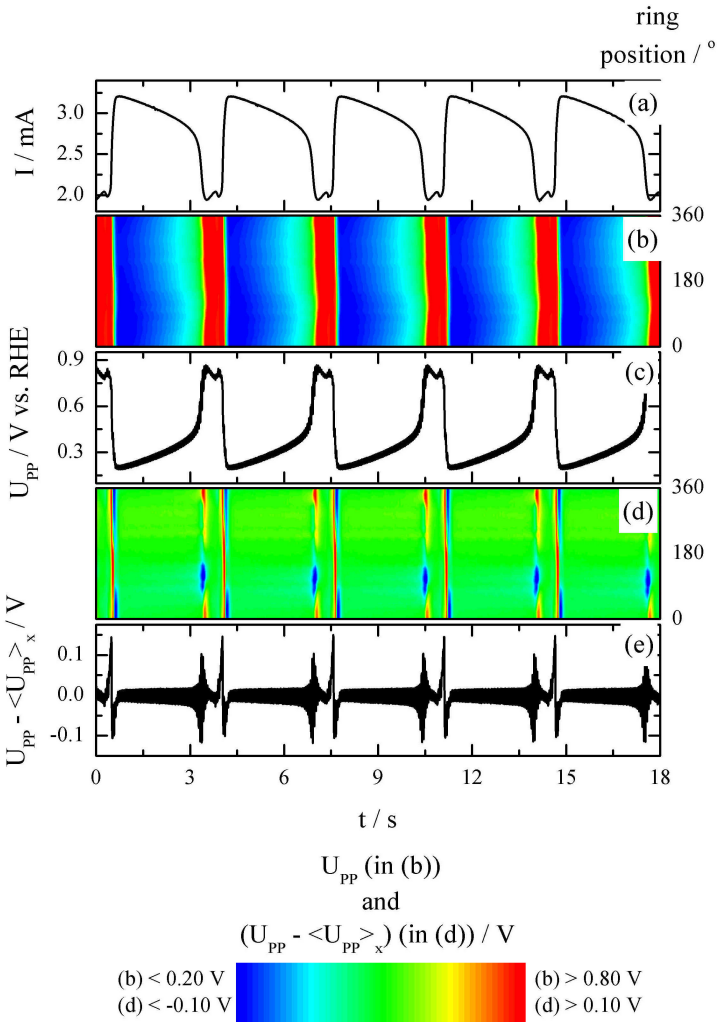

Figure 6.6: (a) I, (c) U_{PP}, and (e) $U_{PP} - \langle U_{PP} \rangle_x$ time series, and the spatiotemporal evolution of (b) U_{PP}, and (d) $U_{PP} - \langle U_{PP} \rangle_x$ as a function of time and ring position for configuration (1) and U = 1.74 V. Remaining conditions as in Figure 6.4.

After this slow relaxation another steep transition now connecting the active to the passive state takes place, and after a small current modulation in the passive region, the cycle starts anew. The spatiotemporal evolution of the interfacial potential, U_{PP}, given in plate (b) shows a nearly homogeneous potential distribution along the ring. However, a spatial symmetry breaking accompanying the fast current transitions is evident in the space-time plots of the inhomogeneous part of the interfacial potential, $U_{PP} - \langle U_{PP} \rangle_x$, as is seen in Figure 6.6 (d). These modulated oscillations (MOs) are qualitatively similar to those already discussed in chapter 5. Such MOs were found in the entire voltage interval and, in the present context, it is enough to bear in mind that the observed patterns under these conditions are completely distinct from those induced by the NGC as discussed next.

Experiments using configurations (2) and (3) and otherwise identical conditions are depicted in Figure 6.7.

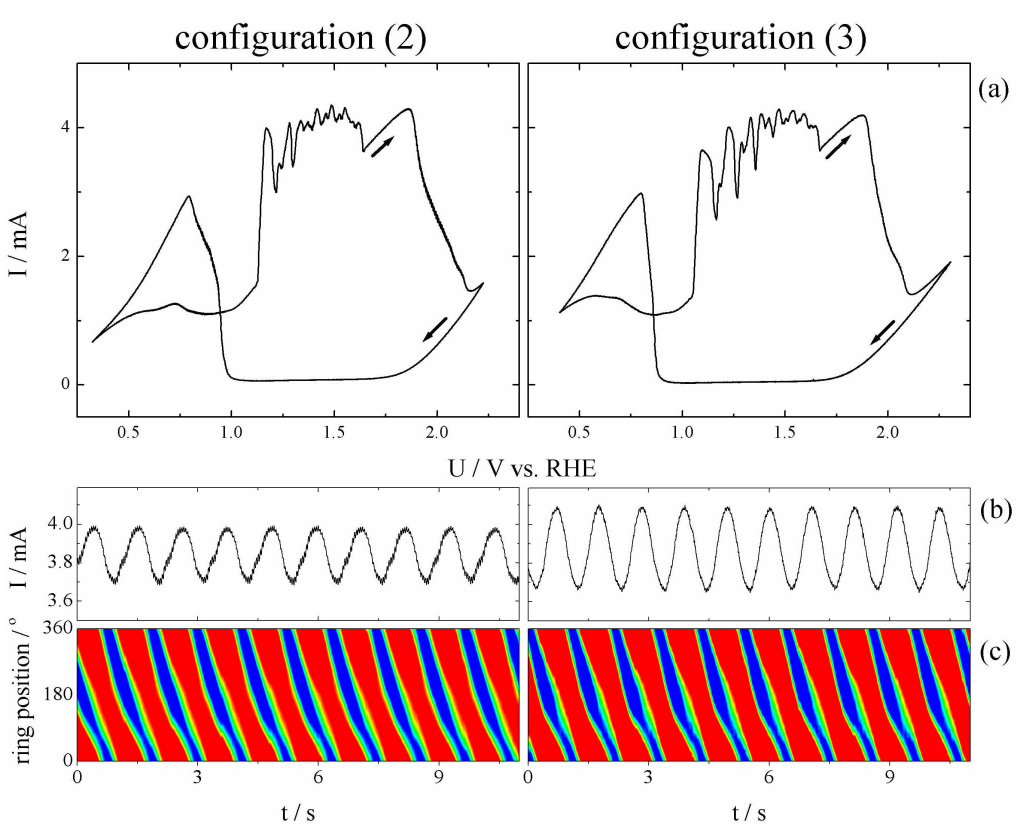

Figure 6.7: (a) Cyclic voltammograms at 0.05 Vs^{-1}; (b) current time series, and the spatiotemporal evolution of (c) U_{PP} - $\langle U_{PP} \rangle_x$ as a function of time and ring position. Experiments carried out using configurations (2) and (3). The applied potential, U, in plots (b) and (c) was 1.44 and 1.51 V in configurations (2) and (3), respectively. $U_{PP} - \langle U_{PP} \rangle_x$ in plots (c) ranges from –0.04 to 0.04 V, and the color scale is from blue to red for both cases. Remaining conditions as given in Figure 6.5.

Cyclic voltammograms, stationary current time series and spatiotemporal distribution of the inhomogeneous part of the interfacial potential for both configurations are presented in Figure 6.7. Quite differently from the CV in Figure 6.5 (curve *i*), current oscillations start after an initial overshooting at ca. 1.1 V and stay rather irregular along the whole oscillatory branch in the I/U curves depicted in Figure 6.7 (a). Fixing the applied potential in the oscillatory region, harmonic small amplitude current oscillations are observed, and typical time series are presented in plates (b) for both configurations. Remarkable is the presence of smaller amplitude oscillations superimposed on the current global oscillations for configuration (2). These small modulations resemble some external noise picked from the network, but actually their frequency coincides with the rotation frequency of the WE (20

Hz) and results from the imperfect placement of the tip of the J-shaped RE with respect to the axis of the WE. Obviously, this additional asymmetric feedback from the potentiostat is absent, when the NID is used, as clearly seen in plate (b) for configuration (3).

The spatiotemporal patterns observed during these harmonic current oscillations are activity pulses of a larger amplitude interfacial potential domain that travels around the ring. Despite the different configurations, the pulse speed is almost identical in situations (2) and (3). The observed harmonic oscillations in the global current result from changes in the width of the pulse during its rotation. Considering that the period with which the pulse width oscillates is identical to the time during which the pulse propagates once around the ring, it is plausible to assume that the current oscillations are due to slight inhomogeneities in the geometrical shape or catalytic activity along the ring [47]. Traveling pulses are common patterns in spatially extended one-dimensional systems with periodic boundary conditions in the presence of negative global coupling and are further discussed in a broader context in chapter 7.

Finally, the almost one-to-one similarity of the spatiotemporal dynamics observed with configurations (2) and (3) represents further evidence that inserting a NID with an absolute resistance R_{NID} between the WE and the potentiostat exerts a negative global coupling of the same magnitude on the system, as a RE that is placed on the central axis of a ring-shaped electrode such that $R_c = -R_{NID}$ [79].

6.4 DISCUSSION

The key result presented in this chapter concerns the experimental proof of the fact that independently of how the compensation is achieved, that is via a Haber-Luggin capillary or via electronic compensation, a NGC is introduced, which strength depends on a combination of the cell resistance, R_Ω, and the compensated resistance, R_c. It implies that whenever the cell resistance is partially compensated, some NGC is induced in the system. The presence of the destabilizing NGC is of utmost importance for the stability of the uniform electrode states [79] and, as further discussed in the next two chapters, it can give rise to several different spatiotemporal patterns.

In the following, some advantages of use of the NID over the use of an adjustable RE as done in previous experiments for the study of the pattern formation in the presence of

NGC are discussed [41, 47, 187]. Although the specific term NID is often used, the following discussion can in principle be extended to any method of electronic compensation.

The most straightforward advantage of using the NID is linked to the fact that it provides an experimentally easier way of adjusting the desired R_c value when compared to the, usually problematic, symmetrical placement of the RE with respect to the WE.

Furthermore, in the case of a two-dimensional WE, the placement of a Haber-Luggin capillary near it implies that the feedback from the potentiostat is asymmetric owing to different distances between different locations of the WE and the tip of the capillary. Such an asymmetry is avoided when the NID is used instead. This is a very important point since an asymmetric placement of the RE may modify the dynamic behavior qualitatively. In this direction, theoretical work by Bîrzu *et al.* [188] revealed an intricate scenario when changing the lateral position of the point RE with respect to the center of a ribbon electrode. The reported behavior includes complex periodic and chaotic motions triggered by the asymmetrical placement of the RE. Hence, the absence of asymmetrical feedback when using the NID points to the possibility of carrying out experiments with two-dimensional electrodes and one-dimensional 'ribbon-like' electrodes overcoming the problem of the asymmetrical coupling. Indeed, the first motivation for using the NID in this context was in order to study the influence of the NGC upon the periodate reduction on rectangular gold electrodes [189].

Another interesting point concerns the possibility of varying the NGC strength up to a larger extent than that feasible with a point RE. As apparent from equation (6.1), the NGC strength is proportional to the ratio of the compensated resistance and the cell resistance, R_c/R_Ω, and by playing with the distance between the RE and the WE, one can face an experimental threshold that limits the achievable R_c. To give a specific example, consider the ring-shaped WE just discussed. In this very case, the distance of 3 mm between RE and WE is already quite near to the closest possible distance, and there was still a considerable amount of uncompensated resistance left due to the radial distance between the tip of the RE capillary and the WE ring. In general, under low conductivity conditions, as typically employed in the experiments described throughout this thesis and previously reported [47] in the $Pt|H_2SO_4,Cl^-,Cu^{2+}|H_2$ oscillatory system, the ratio R_c/R_Ω was never larger than 0.55 when playing with the distance between RE and WE. This problem is absent when electronic compensation is employed. As discussed by Britz [181], it is actually the value of the uncompensated resistance, R_u, that determines whether the entire cell/regulation system will be stable or not,

and the term R_c/R_Ω is not limited by any percentage set *a priori*. The threshold in terms of R_u, at which the system become unstable, depends on the specific system under consideration, as discussed in ref. [181, 185], and it falls in the range of a few ohms. For the typical values of R_Ω in the present system (in the order of 400 to 600 Ω) the ratio R_c/R_Ω can be safely increased up to values close to 1 without any concern about the R_u upper limit. Figure 6.8 illustrates the strength of the NGC, $(R_c/R_\Omega)/(1-R_c/R_\Omega)$ (see equation (6.1)) as a function of R_c/R_Ω. The shaded area accounts for the approximated region of R_c/R_Ω up to the limit of 0.55 discussed above.

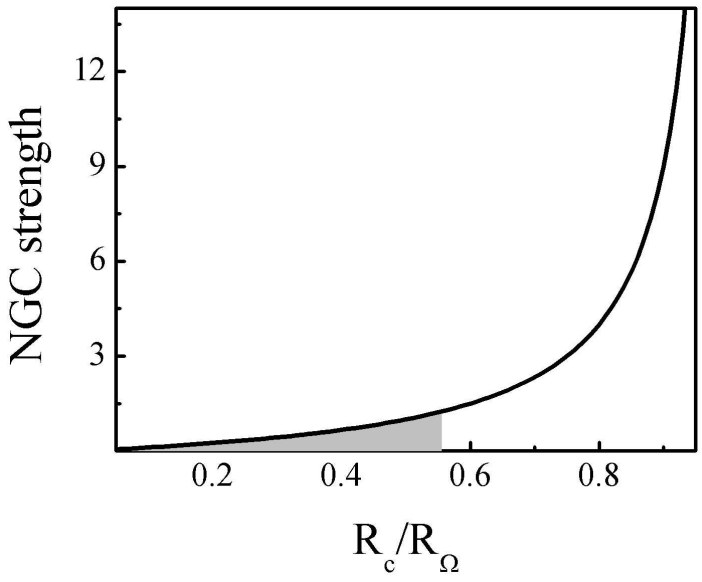

Figure 6.8: Negative global coupling strength (see equation (6.1)) as a function of R_c/R_Ω. Shaded area denotes the approximated region where R_c/R_Ω can be attained when changing the position of the RE with respect to the WE, see text for details.

As clearly seen in this picture, compensating a larger amount of R_c allows the addition of stronger NGC otherwise impossible by reducing the RE/WE distance for this example. In fact, very interesting patterns induced by the presence of strong NGC were obtained at R_c/R_Ω values of about 0.65 as discussed in the next chapter.

The last remarkable point concerns the use of the NID in order to add NGC to (industrial) systems consisting of two electrodes, as recently considered by Krischer [27]. The primary motivation in this sense would be the possibility of taking advantage of carrying out processes under conditions under which patterns form. Specific examples of patterns induced

by the NGC are the traveling pulses depicted above and stationary structures in bistable systems. In both cases the patterned state consists of a coexisting pair of passive and active states. Systems operated under these patterned conditions could be advantageous when compared to the monostable passive state.

6.5 SUMMARY

It has been shown that the negative global coupling introduced into the system depends only on the magnitude of the compensated resistance and the total cell resistance independent of the experimental way in which the compensation is achieved [79]. When compared to the use of a point RE, the use of an electronic ohmic compensation presented some advantages. It allows for:

(a) an easier experimental adjustment of the compensated resistance by just tuning a button;

(b) the absence of an asymmetrical feedback from the potentiostat;

(c) the possibility of compensating a larger part of the total cell resistance;

(d) the addition of NGC to two electrode systems.